Proc. of the 32nd International Symposium on Shock Waves (ISSW32)
doi:10.3850/978-981-11-2730-4_0293-cd

Comparative Study of Linear Interaction Analysis and DNS for Shock-Vorticity Interaction: Scaling of Non-Linear Terms

Pranav Thakare, Yogesh Prasaad M. S., Krishnendu Sinha, Vineeth Nair
Department of Aerospace Engineering, Indian Institute of Technology Bombay, Mumbai, 400 076, India

Corresponding author's name: Krishnendu Sinha, krish@aero.iitb.ac.in

Abstract

Interaction of shock waves with turbulence is a complex problem in high-speed flows. Linear interaction analysis (LIA) is a theoretical tool used to predict the shock-induced turbulence amplification. It is based on the elementary interaction of a two-dimensional disturbance wave with a normal shock. In this work, we assess the accuracy of LIA when compared to high-order numerical simulation of shock-vorticity wave interaction. We present results for a range of upstream wave amplitudes and orientations, at different shock Mach numbers. The deviation between LIA and DNS is, as expected, a strong function of wave inclination angle and mean flow Mach number. We perform second-order error analysis using Rankine-Hugoniot relations to find scaling parameters that can characterize these deviations. We find that the deviations scale with the square of the sine of the downstream vorticity wave angle at a given Mach number and with the square of the mean compression ratio across the shock at a given upstream incidence angle.

1 Introduction

Shock waves in a turbulent flow is one of the most critical problems in high-speed flow dynamics. The turbulent fluctuations are largely modified by the shock wave upon interaction and in return, the structure of the shock is distorted by the turbulence. The interaction between turbulence and shock has been studied by researchers for many years using experimental, theoretical and numerical studies. Experiments are limited due to the difficulties in setting up a clean environment, where only the effects of the turbulence and the shock wave can be isolated. Theoretical and numerical approaches are commonplace for investigating shock-turbulence interaction.

Turbulence in a compressible flow can be represented as a linear combination of three fundamental modes—vorticity, entropy and acoustic—under the condition that the fluctuation levels are small compared to the mean flow [1]. The vorticity mode is related to the solenoidal velocity fluctuations in the flow and the entropy mode to the density and temperature fluctuations. The acoustic mode comprises pressure fluctuations, irrotational velocity fluctuations and the isentropic components of density and temperature fluctuations. The theoretical method called linear interaction analysis (LIA) utilizes this decomposition to investigate shock-turbulence interaction. In LIA, the fundamental modes defined by Kovásznay [1] are represented as wave disturbances, which are then extended to explain the complete shock-turbulence interaction problem.

Development of the LIA theory dates back to the mid of the 20$^{\text{th}}$ century, when Moore [2] and Ribner [3] independently laid the base of LIA theory. Moore [2] studied the unsteady interaction of an acoustic wave with a normal shock and Ribner [3] investigated the interaction of a vorticity wave with a normal shock. Chang [4] supplemented LIA theory by providing the necessary expressions for the case of entropy disturbances interacting with a normal shock. McKenzie and Westphal [5] later analyzed the linear effects of small amplitude fluctuations in the flow interacting with an oblique shock.

In recent times, LIA has been used extensively to investigate the physical mechanisms responsible for turbulence amplification at a shock wave. Mahesh *et al.* [6] analyzed the interaction of combined vorticity and entropy disturbances with a normal shock, where the effect of upstream entropy fluctuations on the post-shock flow-field is emphasized. Subsequently, Fabre *et al.* [7] analyzed the interaction of an entropy spot with a normal shock using LIA, where elementary waves of entropy fluctuations were used to construct the entropy spot. A similar approach was followed by Griffond [8] to study the effect of a mixture of gases composed of elementary waves of fluctuating concentration with a normal shock. Recently, Quadros *et al.* [9] investigated the turbulent energy flux generated by a normal shock using LIA.

The alternate approach to analyze shock-turbulence interaction is by numerical simulations. Zang *et al.* [10] compute the solutions for planar waves of each of the fundamental Kovásznay modes interacting with normal shocks of varying strengths. Their analysis was restricted to incident waves making an angle of 30° with the shock-normal direction. Mahesh *et al.* [6] investigated acoustic and vorticity-entropy waves, each interacting individually with a normal shock using direct numerical simulations. Results from the computations, such as turbulent kinetic energy (TKE) and vorticity variances, were found to match qualitatively with results from LIA. Recently, the works of Larsson *et al.* [11, 12], Ryu and Livescu[13, 14], Quadros *et al.* [9, 15], Tian *et al.* [16] and Sethuraman *et al.* [17] compare various second-moment statistics obtained from DNS with LIA, and find good match for cases with low turbulent Mach number (M_t).

It is generally accepted that LIA results are valid in the limit of vanishing turbulent Mach number and infinite Reynolds number. Much of the comparisons of LIA and DNS, either for varying M_t [13] or by artificially removing viscous dissipation [12], show this qualitative trend. However, very few quantitative estimates exist for the bounds of validity of LIA. The question as to within what range of governing parameters the results from LIA can be considered reliable is still open. This question has become particularly relevant in recent times, where LIA is increasingly being used as a surrogate to numerical simulation in regions of shock waves [18], and LIA-based turbulence models are increasingly being used in practical applications [19].

In this paper, we attempt to address the validity of LIA vis-a-vis DNS from a fundamental perspective. We consider the elementary interaction of a single vorticiity wave with a normal shock, and arrive at quantitative estimates of error in LIA when compared to numerical simulations. We perform controlled numerical simulations by systematically varying the amplitude and orientation of the wave and the shock Mach number, and compare the solution with LIA predictions for identical parameter values. Euler simulations are performed, so as to isolate the non-linear effects inherent in shock-turbulence interaction. We also derive an error estimate from the governing equations using linear analysis.

2 Methodology

2.1 Linear Interaction Analysis

Let us consider a two-dimensional planar vorticity wave with its wavenumber vector $\vec{k}$ inclined at an angle α with the x axis (streamwise direction). Mathematically, the vorticity wave can be represented as

$$\Omega' = \epsilon e^{i(\vec{k}.\vec{r}-\omega t)}, \tag{1}$$

where Ω' is the non-dimensional vorticity fluctuation, $\vec{r}$ is the position vector, and $\vec{k}$ represents the wavenumber vector of the upstream vorticity fluctuations. The amplitude of the upstream velocity fluctuations is denoted by ϵ and the time variation is given in terms of the temporal frequency, ω. The vorticity wave is being convected by a one-dimensional (1D) uniform mean flow of velocity $\overline{U}_1$ towards the normal shock located parallel to the y-axis. The shock deforms in response to the fluctuations and the position of the unsteady shock is given by the function $\xi(y,t)$.

The incident vorticity wave is refracted, whereas acoustic and entropy waves are generated at the shock. The generated acoustic wave and the vorticity/entropy wave are inclined at angles α^p and α^s respectively in the downstream region. The refracted vorticity wave is aligned in the same direction as that of the entropy wave. The wavenumber vector of the acoustic wave is represented by $\vec{k^p}$ and that of the non-acoustic waves (vorticity and entropy) is given by $\vec{k^s}$. The post-shock acoustic wave can be either propagating or decaying depending on the angle of the incident wave. There exists a critical angle, α_c for $\alpha \in [0, \pi/2]$, beyond which the acoustic waves decay immediately behind the shock.

The linearized Euler equations with the linearized Rankine-Hugoniot (R-H) conditions as the boundary conditions at the shock are solved to obtain post-shock wave characteristics. The dispersion relation at the shock constrained by the continuity equation yields the transverse (y-direction) wavenumber ($k_y^{s/p}$) and the temporal frequency (ω) of the wave to be the same as the incident wave. The streamwise (x-direction) wavenumber of the non-acoustic wave (k_x^s) is compressed by a factor of mean velocity jump ($\overline{U}_1/\overline{U}_2$) across the shock, whereas the corresponding wavenumber for the acoustic wave (k_x^p) is determined by the acoustic wave equation. The linearized R-H conditions relating the downstream fluctuations in terms of upstream fluctuations are substituted in the linearized Euler equations to obtain the amplitudes of the disturbance waves (Z_{vv}, Z_{vx}, Z_{vp} and Z_{vs}) for the region behind the shock. The amplitudes of the waves are functions of the shock strength (M_1), incidence angle (α) and the adiabatic index (γ). The reader is directed to Fabre *et al.* [7] for a complete description.

2.2 Numerical analysis

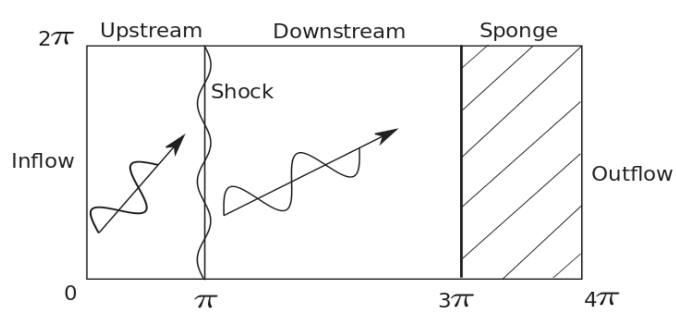

Fig. 1 A schematic of the numerical domain showing the planar wave interaction with a normal shock wave

Interaction of a vorticity wave with a normal shock is simulated numerically by solving the compressible Euler equations for a perfect gas with $\gamma = 1.4$. The flow variables are normalized such that the upstream velocity is equal to the upstream Mach number, by using upstream values of density and sound speed as the normalizing variables. A fifth-order accurate WENO scheme with Roe-flux splitting is used to calculate the approximate fluxes near the shock and a sixth-order accurate central difference scheme is used for the remainder of the domain. The numerical shock is captured using a modified Ducros sensor [12].

Computations are carried out over the 2-dimensional grid shown in Fig. 1. The length of the domain is 4π in the streamwise direction and 2π in the transverse direction. A grid size of 400×64 is found to be suitable after a thorough grid independence test, and is used for all the cases considered here. Supersonic boundary condition is used at the inflow ($x = 0$) and a non reflecting subsonic boundary condition is used at outflow ($x = 4\pi$). Periodic boundary condition is used in the transverse direction. The normal shock located initially at $x = \pi$ oscillates along the transverse direction due to upstream fluctuations. A time dependent backpressure controller is used to keep the shock stationary in the domain similar to the procedure used in [12, 17].

The flow downstream of a normal shock is subsonic which allows acoustic waves from the outflow to propagate towards the shock. These acoustic reflections are undesirable and are to be damped/avoided. A numerical sponge is used to achieve this, which dampens the fluctuations to a target state defined by the Rankine-Hugoniot conditions.

3 Results and Discussion

Interaction of a vorticity wave with a normal shock is investigated for a flow with $M_1 = 1.5$ using LIA and numerical simulations (hereafter referred as DNS). The amplitude and incidence angle of the incoming waves are varied keeping the upstream shock-parallel wavenumber k_y at a fixed value of 2.

The instantaneous vorticity profiles excluding the sponge region are compared between LIA and DNS at the $y = 0$ location for two different incident angles and amplitude levels (see Fig. 2). The profiles are extracted at the end of one wave cycle after the initial transients have passed, which is identified by the change in mean shock speed in the domain. The chosen incidence angles are in the propagating regime of the downstream acoustic waves, and the maximum amplitude ($\epsilon = 10\%$) is marginally in the linear limit. The mean shock position is shown by a vertical dotted line in the figures.

The compressive action of the normal shock amplifies the vorticity, and this amplification increases as the incoming wave amplitude, ϵ increases. The wavelength of the vorticity wave decreases across the shock, and is a function of the incidence angle α. This is evident from Figs. 2a and 2c, where the reduction in wavelength of the downstream vorticity wave is relaxed as the incidence angle is increased. Symbols overlapping on the lines for $\alpha = 30°$ indicate that there is an excellent match of the wave characteristics (wavenumber and inclination angle) between DNS and LIA profiles.

LIA predicts sinusoidal patterns for the downstream waves, whereas DNS shows an approximate sinusoidal pattern. For incidence angle of $\alpha = 30°$, there is negligible phase difference between LIA and DNS profiles throughout the downstream region. This is not the case for the high incidence angle of $\alpha = 55°$, where there is a noticeable phase difference between LIA and DNS profiles in the region close to the end of the domain. In the region immediately behind the shock, the phase difference is found to be negligible.

The phase difference becomes larger for higher values of ϵ as seen in the insets of Figs. 2c and 2d.

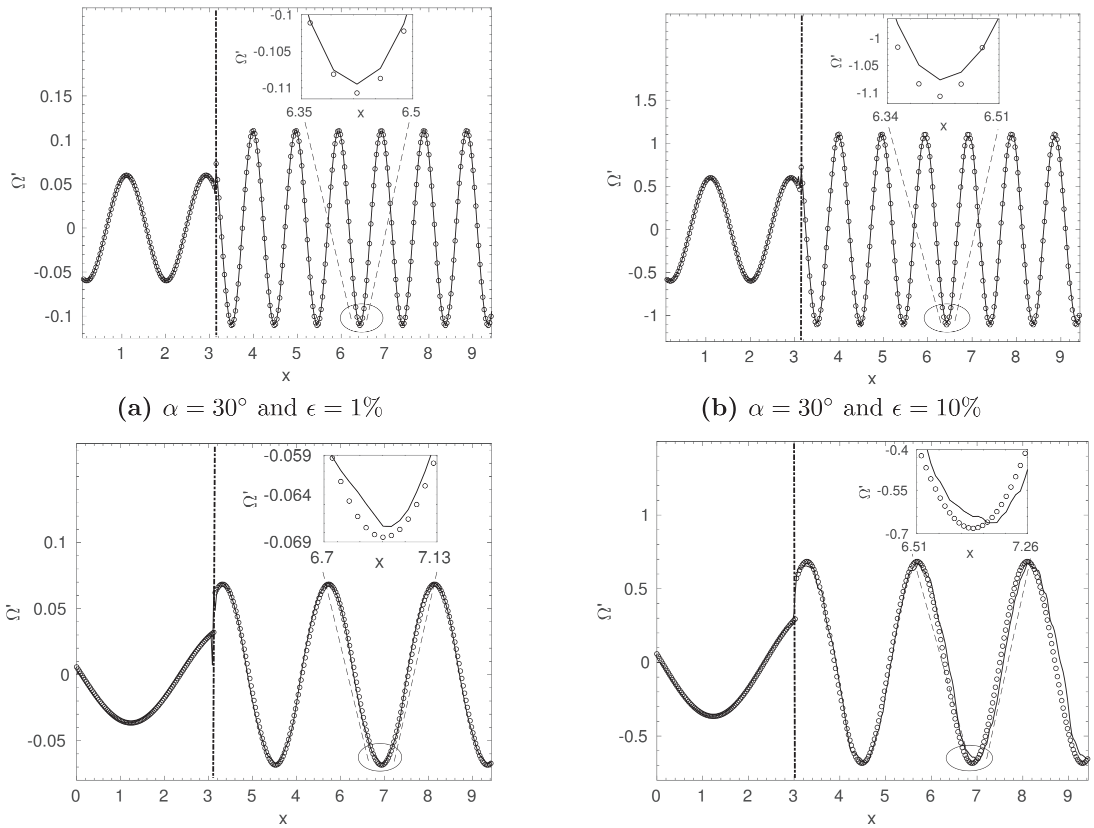

(a) $\alpha = 30°$ and $\epsilon = 1\%$ **(b)** $\alpha = 30°$ and $\epsilon = 10\%$

(c) $\alpha = 55°$ and $\epsilon = 1\%$ **(d)** $\alpha = 55°$ and $\epsilon = 10\%$

Fig. 2 Comparison of LIA and DNS vorticity profiles for two different incidence angles ($\alpha = 30°$ and $55°$) and amplitude levels ($\epsilon = 1\%$ and 10%). DNS profiles are shown by solid lines and LIA profiles are shown by circles. The insets show a magnified portion of the downstream region indicating the difference between the LIA and the DNS profiles

3.1 RMS Error

A measure of the deviation of LIA from DNS is studied using the idea of root mean square error (E_{rms}). The RMS error is calculated over the downstream region till the start of the sponge region. It is expressed as,

$$E_{rms} = \sqrt{\frac{1}{N}\sum_{n=1}^{N}(\Omega'_{DNS} - \Omega'_{LIA})^2}, \tag{2}$$

where Ω'_{DNS} and Ω'_{LIA} represent the non-dimensional vorticity fluctuations obtained from the numerical simulations and LIA, respectively. Here, N is the number of grid points used to compute the E_{rms} in the downstream region. The number of grid points were found to be sufficiently large for statistical convergence.

Figure 3a shows the E_{rms} evaluated for different α values, varying from 30° to 50° for $M_1 = 1.5$ flow. We observe that E_{rms} increases with ϵ as well as with α. Variation of

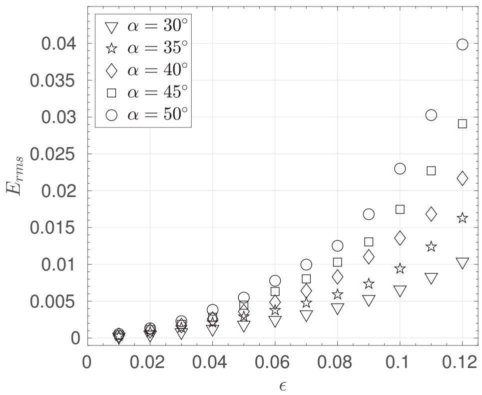

(a)

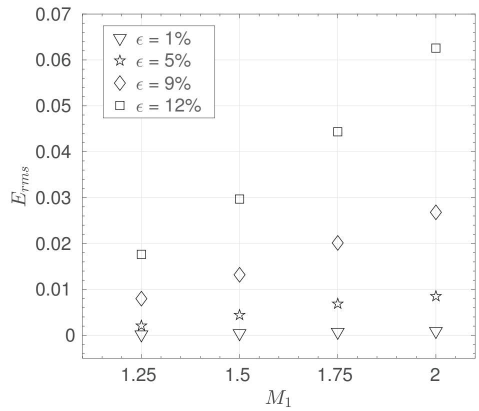

(b)

Fig. 3 Variation of E_{rms} averaged over the downstream region (a) against ϵ for different α values, and (b) against M_1 for different ϵ values

E_{rms} with respect to ϵ for a particular α value is found to be super-linear or quadratic at the most. This implies that non-linear effects become more prominent as ϵ is increased. Additional deviation is observed on top of the effect of ϵ for increasing values of α towards the critical angle.

The deviation between LIA and DNS profiles for varying M_1 and ϵ values is shown in Fig. 3b. The Mach number is varied from 1.25 to 2 for $\alpha = 45°$ case. Variation of E_{rms} with respect to M_1 appears to be linear for a particular ϵ value. In the next section, we investigate these variations by computing the non-linear terms in the R-H conditions.

3.2 Error analysis

We decompose the R-H conditions into their mean and fluctuating components in the frame of reference attached to the instantaneous shock wave. We retain the first and the second order terms in fluctuations, whereas the mean and the other higher order terms are neglected. This is under the assumption that the differences between the numerical simulations and the LIA are mostly due to the second order terms.
Mass Conservation:

$$\frac{(u_1' - \xi_t)}{\bar{U}_1} = \frac{(u_2' - \xi_t)}{\bar{U}_2} + \frac{\rho_2'}{\bar{\rho}_2} + \frac{\rho_2'}{\bar{\rho}_2}\frac{(u_2' - \xi_t)}{\bar{U}_2}, \tag{3}$$

Streamwise momentum conservation:

$$\frac{rp_1'}{\bar{\rho}_1\bar{U}_1^2} + \frac{2r(u_1' - \xi_t)}{\bar{U}_1} + \frac{r(u_1' - \xi_t)^2}{\bar{U}_1^2} = \frac{p_2'}{\bar{\rho}_2\bar{U}_2^2} + \frac{2(u_2' - \xi_t)}{\bar{U}_2} + \frac{(u_2' - \xi_t)^2}{\bar{U}_2^2} + \frac{2\rho_2'}{\bar{\rho}_2}\frac{(u_2' - \xi_t)}{\bar{U}_2} + \frac{\rho_2'}{\bar{\rho}_2}, \tag{4}$$

Transverse momentum conservation:

$$\frac{rv_1'}{\bar{U}_1} - r\xi_y - \frac{r\xi_y u_1'}{\bar{U}_1} = \frac{v_2'}{\bar{U}_2} - \xi_y - \frac{\xi_y u_2'}{\bar{U}_2}, \tag{5}$$

Energy conservation:

$$\frac{r^2\bar{U}_1(u_1'-\xi_t)}{\bar{U}_1^2}+\frac{r^2(u_1'-\xi_t)^2}{\bar{U}_1^2}=\frac{C_pT_2'}{\bar{U}_2^2}+\frac{\bar{U}_2(u_2'-\xi_t)}{\bar{U}_2^2}+\frac{(u_2'-\xi_t)^2}{\bar{U}_2^2}, \tag{6}$$

where u', ρ', T' and ξ_y represent the fluctuations in velocity, density, temperature and shock-corrugation slope, respectively. Here, $r=\bar{U}_1/\bar{U}_2$ is the velocity jump across the shock. Note that $\rho_1'=p_1'=T_1'=0$ for the case of vorticity wave considered here.

We follow a weakly non-linear approach, where the second order terms are constructed using the linearized expressions for the fluctuations obtained using LIA. This is based on the assumption that the exact second order terms are approximately equal to the product of their linear counterparts. The second order terms from the R-H conditions that contribute to non-linear vorticity generation downstream of the shock are listed below.

$$E_{II}(\epsilon,\alpha,M_1)=\Bigg[\underbrace{\frac{(u_2'-\xi_t)^2}{\bar{U}_2^2}}_{\psi_1}+\underbrace{\frac{2\rho_2'}{\bar{\rho}_2}\frac{(u_2'-\xi_t)}{\bar{U}_2}}_{\psi_2}-\underbrace{\frac{\xi_y u_2'}{\bar{U}_2}}_{\psi_3}\Bigg], \tag{7}$$

quantifies the non-linear effect in vorticity fluctuations due to the second order terms. Here, ψ_1, ψ_2 and ψ_3 are the dominant terms taken from the R-H conditions. Complete expressions for the linear terms, $u_2'/\bar{U}_2$, $\rho'/\bar{\rho}_2$ and $\xi_t/\bar{U}_2$ can be found in Fabre et al. [7].

3.3 Scaling Parameters

We study the effect of $\psi_i=f(\epsilon,\alpha,M_1)$ for $i=1,2,3$ in Eq. (7) on the rms error (E_{rms}). Variation of ψ_i with respect to α and M_1 is shown in Figs. 4a and 4b, respectively with ψ_i^* denoting the complex conjugate of ψ_i.

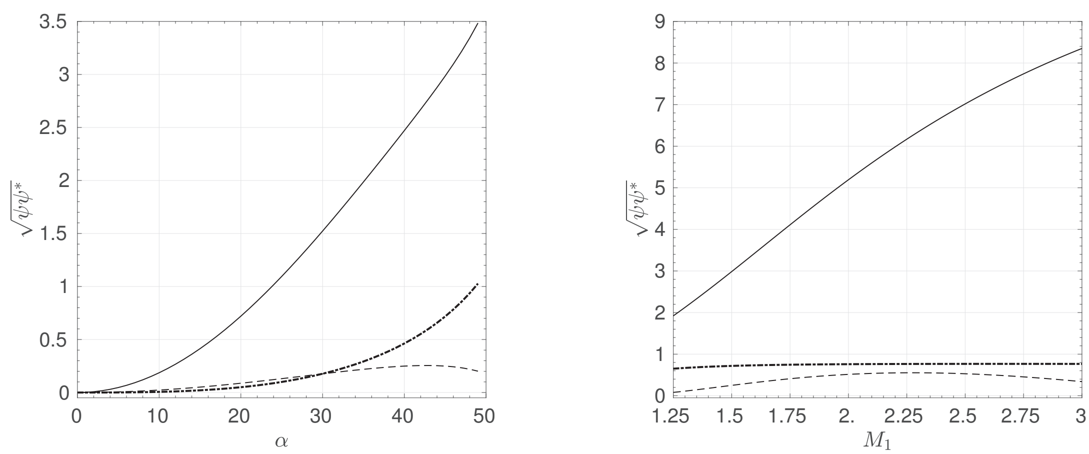

(a) **(b)**

Fig. 4 Variation of $\sqrt{\psi_1\psi_1^*}$ (solid line), $\sqrt{\psi_2\psi_2^*}$ (dashed line), and $\sqrt{\psi_3\psi_3^*}$ (dotted line) against (a) different incidence angles (α) for $M_1=1.5$ and (b) different M_1 for $\alpha=45°$

We notice that ψ_1 is the most dominant term in E_{II}, which is considered for further study. The ψ_1 term is expanded as follows

$$\psi_1=\frac{(u_2'-\xi_t)^2}{\bar{U}_2^2}\quad\approx\epsilon^2\bigg(\sin^2\alpha^s Z_{vv}^2+2ir\sin\alpha^s\cos\alpha Z_{vv}Z_{vx}-r^2\cos^2\alpha Z_{vx}^2\bigg), \tag{8}$$

where only the vortical component of the velocity fluctuations is considered [7].

We systematically study the contribution of the different terms from ψ_1 over a range of Mach number and upstream wave angle. The motivation is to understand the effect of the important physical parameters of the problem on the rms error via the ψ_1 term. The different terms in Eq. (8) consist of the product of transfer function Z and functions of wave angles α and α^s. The transfer functions and the downstream vorticity wave angle α^s have non-trivial dependence on the Mach number and other governing parameters. We use LIA solution to compute the contribution of the transfer functions and the α-terms to the overall error. It is found that $\sin^2\alpha^s$ from the first term in Eq. (8) has a dominant effect, and it gives the correct qualitative variation of the rms error observed in Fig. 3a. Normalizing E_{rms} with $\sin^2\alpha^s$ shows excellent collapse of the data, thereby essentially eliminating the variation with incidence angle for a fixed shock Mach number. This implies that rms error in the vorticity wave computed using LIA, as compared to DNS, scales as $\sin^2\alpha^s$.

In a similar procedure, we attempt to find the relation between M_1 and E_{rms} via the r^2 term, which is the preceding coefficient in the third sub-term of the ψ_1 term given in Eq. (8). Normalization by r^2 collapses the E_{rms} variation to a single curve (approximately) as shown in Fig 5b. Thus, we find that the variation of E_{rms} against M_1 for a particular ϵ value scales as r^2.

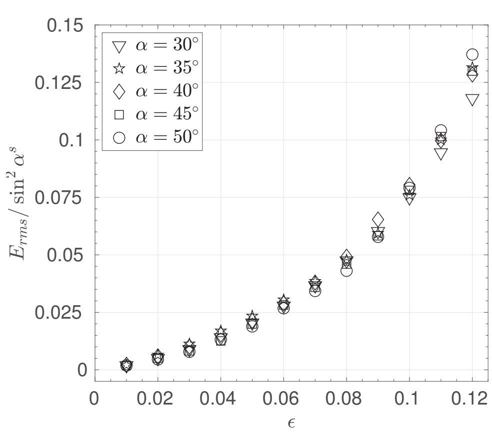

(a)

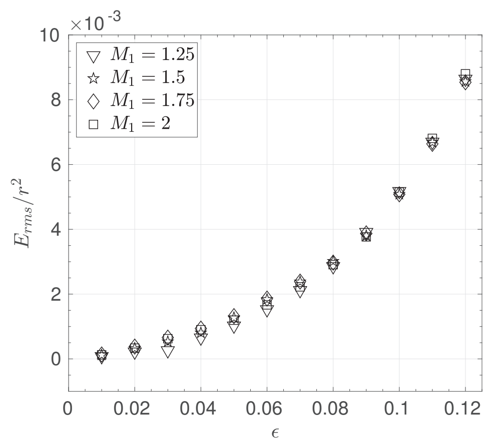

(b)

Fig. 5 Variation of scaled E_{rms} against ϵ for different incidence angles and flow Mach numbers: (a) Case of $M_1 = 1.5$ with scaling parameter $\sin^2\alpha^s$, (b) Case of $\alpha = 45°$ with scaling parameter r^2

4 Conclusion

In this paper, we present results from numerical simulations and linear interaction analysis of a two-dimensional planar vorticity wave interacting with a normal shock. The linear theory is based on Kovásznay mode decomposition of the disturbance field, and we focus on the amplification of the incident vorticity wave by the shock wave. A high-order numerical method, along with carefully tailored boundary conditions, is used to get accurate solutions for a range of Mach numbers, upstream wave amplitudes and inclination angles. As expected, the solution from linear theory matches the nonlinear simulations for low wave amplitudes, up to about 5%. The deviation between LIA and DNS (E_{rms}) increases significantly with increasing wave inclination angle, and the shock Mach number.

We present a weakly nonlinear analysis of the Rankine-Hugoniot jump conditions at the shock to compute the magnitude of the second-order error terms that contribute to the deviation. It is found that the variation of E_{rms} scales with the square of the sine of the downstream vorticity wave inclination angle, at a given Mach number. At a constant upstream incidence angle, E_{rms} is found to increase as the square of the mean density ratio across the shock wave for increasing Mach numbers.

References

[1] L. S. G. Kovásznay, J. Aeronaut. Sci. **20**, 657 (1953)

[2] F. K. Moore, NACA TR 1165, 217 (1954)

[3] H. S. Ribner, NACA TR 1164, 199 (1954)

[4] C. -T. Chang, J. Aeronaut. Sci., **24**, 675 (1957)

[5] J. F. McKenzie, K. O. Westphal Phys. Fluids, **11**, 2350 (1968)

[6] K. Mahesh et al., *The interaction of a shock wave with a turbulent shear flow*, (Stanford University Report No. TF-69, California, 1996), pp. 45–87

[7] D. Fabre et al., *Linear interaction of a cylindrical entropy spot with a shock*, Phys. Fluids. **13**, 2403 (2001)

[8] J. Griffond, Phys. Fluids. **17**, 086101 (2005)

[9] R. Quadros et al., *Turbulent energy flux generated by shock/homogeneous-turbulence interaction*, J. Fluid. Mech. **796**, 113 (2016)

[10] T. A. Zang et al., *Numerical Computations of Turbulence Amplification in Shock-Wave Interactions*, AIAA J. **22**, 13 (1984)

[11] J. Larsson, S. K. Lele Phys. Fluids. **21**, 126101 (2009)

[12] J. Larsson et al., *Reynolds-and Mach-number effects in canonical shock-turbulence interaction*, J. Fluid Mech. **717**, 293 (2013)

[13] J. Ryu, D. Livescu J. Fluid Mech. **756**, R1 (2014)

[14] D. Livescu, J. Ryu Shock Waves. **26**, 241 (2016)

[15] R. Quadros et al., *Kovasznay Mode Decomposition of Velocity-Temperature Correlation in Canonical Shock-Turbulence Interaction*, Flow, Turbul. and Combust. **97**, 787 (2016)

[16] Y. Tian et al., *Numerical study of variable density turbulence interaction with a normal shock wave*, J. Fluid Mech. **829**, 551 (2017)

[17] Y. P. M. Sethuraman et al., *Thermodynamic fluctuations in canonical shock–turbulence interaction: effect of shock strength*, Theor. Comput. Fluid Dyn. **32**, 629 (2018)

[18] N. O. Braun et al., *Large eddy simulation investigation of the canonical shock-turbulence interaction*, J. Fluid Mech. **858**, 500 (2019)

[19] S. Roy et al., *Variable Turbulent Prandtl Number Model for Shock / Boundary - Layer Interaction*, AIAA J. **56**, 342 (2018)